Synchronous Waveform Measurements to Locate Transient Events and Incipient Faults in Power Distribution Networks

Milad Izadi, *Student Member, IEEE*, and Hamed Mohsenian-Rad, *Fellow, IEEE*

***Abstract*—A new method is proposed to identify the location of transient events, including incipient faults, in power distribution systems, by using synchronized measurements from an emerging class of sensors, called *waveform measurement units* (WMUs). WMUs capture the voltage and current waveforms in time domain. The proposed method consists of three steps. The first step is to characterize the oscillatory modes of the transient components of all the captured synchronized voltage and current waveforms from all WMUs, by conducting a multi-signal modal analysis. The second step is to construct a circuit model for the underlying distribution feeder at the identified dominant mode(s) of the transient event. The final step is to identify the location of the transient event with the means of a method that involves certain forward and backward analyses of the constructed circuit model. The proposed method requires installing as few as only two WMUs. It can also utilize several synchronized waveform measurements when several WMUs are available. The performance of the proposed method is assessed on the IEEE 33-bus test system; for different cases of transient events, such as sub-cycle incipient faults, multi-cycle incipient faults, permanent faults, as well as benign yet informative events such as capacitor bank switching. Both the accuracy and the robustness of the proposed method are verified. The analysis and results in this paper provide new insights on possible applications of synchronized WMU measurements; while they also address a highly challenging problem in power distribution networks.**

***Index Terms*—Waveform measurement unit, synchronous waveforms, WMU, transient event, location identification, sub-cycle and multi-cycle incipient faults, data-driven method, modal analysis.**

I. Introduction

TRANSIENT events occur frequently in power distribution systems due to various changes in system conditions. Transient events have short duration but sometimes large magnitude. Examples of transient events include incipient faults and switching events. An incipient fault occurs in a distribution feeder when there is a crack in the insulation of an equipment, e.g., a cable, which ignites an electric arc [1]. Incipient faults are typically *self-clearing* faults and have short duration, ranging from a quarter of a cycle (sub-cycle), to up to four cycles (multi-cycle) [2]. That is why incipient faults are *difficult* to analyze. It is critical to detect and locate incipient faults in power distribution systems to prevent future permanent faults.

In this paper, we seek to identify the location of transient events in power distribution systems by using *synchronized voltage and current waveform measurements*. Such measurements are provided by *waveform measurement units* (WMUs), which are an emerging class of sensors [3], [4]. They provide precise GPS-synchronized *voltage and current waveforms* in time domain [5], [6]. A typical WMU can report 256 readings per cycle. In order to support synchronized waveform measurements at such high reporting rate, WMUs have a time accuracy of 1 μsec [7]. So far, WMUs have been used in *a few* applications, such as to study harmonic addition and cancellation in transformers [3]; to analyze sub-synchronous resonance [8]; to locate power quality events [4]; and to achieve situational awareness [5], [6].

A. Motivation: D-PMUs Versus WMUs

The waveform measurements from WMUs are well-suited to study transient events in power distribution systems, in particular, when we compare them with the phasor measurements from distribution-level phasor measurement units (D-PMUs); a.k.a, micro-PMUs, which are another emerging class of sensors [9].

Fig. 1 shows an example of an incipient fault that occurs on a power distribution system, and the corresponding *current phasors* that are captured by two D-PMUs as well as the *current waveforms* that are captured by two WMUs. D-PMU 1 and WMU 1 are installed at the beginning of the feeder; and D-PMU 2 and WMU 2 are installed at the end of the feeder.

The incipient fault causes very small changes in the phasor measurements of the D-PMUs, see Figs. 1(b) and (c). The exact shape of such small changes depends on the internal filtering, the size of the measurement window, and other dynamic characteristics of the D-PMUs. Importantly, these small changes in synchrophasors are *not* much informative; because they appear just like a normal variation in current, as opposed to an indication of an incipient fault. In a sharp contrast, the impact of the incipient fault is clearly visible in

Manuscript received August 29, 2020; revised March 12, 2021; accepted May 8, 2021. Date of publication May 17, 2021; date of current version August 23, 2021. This work was supported in part by UCOP under Grant LFR-18-548175. Paper no. TSG-01323-2020. *(Corresponding author: Hamed Mohsenian-Rad.)*

The authors are with the Department of Electrical and Computer Engineering, University of California at Riverside, Riverside, CA 92507 USA (e-mail: mizadi@ece.ucr.edu; hamed@ece.ucr.edu).

Color versions of one or more figures in this article are available at https://doi.org/10.1109/TSG.2021.3081017.

Digital Object Identifier 10.1109/TSG.2021.3081017

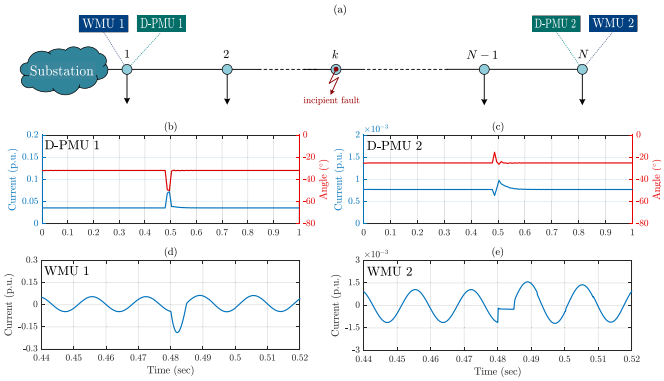

Fig. 1. An example for a sub-cycle incipient fault on a distribution feeder that is seen by two D-PMUs versus by two WMUs: (a) the locations of the sensors; (b)-(c) synchronized current phasor measurements from the two D-PMUs; (d)-(e) synchronized current waveform measurements from the two WMUs.

the waveform measurements of the two WMUs, see Figs. 1(d) and (e).

B. New Approach and Contributions

Motivated by examples such as the one in Section I-A, our goal in this paper is to use the synchronized voltage and current waveforms from WMUs to identify the location of transient events, such as incipient faults, in power distribution systems. The contributions of this paper are as follows:

1) On one hand, this paper introduces a new use case for WMUs, as an emerging smart grid sensor technology. On the other hand, this paper addresses a challenging problem in power distribution systems. Here, our focus is specifically on transient events; which are *inherently very short in duration*. Identifying the location of such short events is very challenging. Nevertheless, the proposed method can identify the correct location in most cases.
2) The proposed method is applicable to different types of transient events, such as sub-cycle and multi-cycle incipient faults. This is a direct result of using the synchronized waveform measurements, as opposed to using synchronized phasor measurements as in other methods, e.g., in [10], which cannot suitably observe transient events.
3) The proposed method takes advantage of the availability of synchronized waveform measurements from multiple WMUs; as opposed to the common approach in the existing incipient fault location methods that work based on measurements from one sensor. Furthermore, unlike the existing incipient fault location methods, such as in [11], the proposed method considers the fact that there are loads between the sensor location and the fault location.
4) The proposed method works for two fundamentally different types of transient events: the events that are static in nature, such as in case of arcs in incipient faults that are resistive and do *not* create any new oscillation mode; as well as the events that are dynamic in nature, such as in case of capacitor bank switching that is reactivate and create new oscillation mode(s) in the system.
5) The proposed method is also able to pin-point the correct location of *permanent events*, such as permanent faults and capacitor bank switching events. The advantage here is that the proposed method is prompt because there is no need to wait until the system reaches steady-state conditions before we can identify the location of the event.

C. Related Literature

The majority of the existing methods in the area of event and fault location identification use measurements that are meant for steady-state analysis, such as phasor measurements, which are suitable only to analyze permanent events and faults, e.g., see the impedance-based methods in [12]–[14] and the wide area-based methods in [10], [15], [16]. As we saw in the example in Section I-A, phasor measurements cannot accurately capture short transient events, such as incipient faults.

There is a limited literature on incipient fault location identification using waveform measurements, e.g., in [11], [17]–[23]. The methods in these papers use waveform measurements from one sensor to estimate the *distance* between the fault location and the sensor location. Their accuracy decreases when there are loads between the fault location and the sensor location; which is often the case in power distribution feeders. This issue can be alleviated by using a load compensation strategy [21]. Also, they may not work well with locating sub-cycle incipient faults; because of the extremely short duration of the fault.

There are also a few studies that address location identification for benign events, such as capacitor bank switching, using waveform measurements from one sensor, e.g., see [24], [25], where the proposed methods are distance-based methods. A new concept, called the synchronized Lissajous curve, is introduced in [5], [6] that provides clear insight about the location of events using waveform measurements from as few as only two WMUs.

Compared to the preliminary conference version of this work in [4], the current journal submission has several new and important contributions. First and foremost, the method in [4] was limited to the study of capacitor bank switching. It did *not* address incipient faults; which is the primary focus in this manuscript. Incipient faults have much shorter duration, as short as only a quarter of a cycle; therefore, they are much more challenging to identify their location compared to capacitor bank switching events. Furthermore, here we use multi-signal modal analysis that is particular suitable for the type of method in this paper, as opposed to the single-signal modal analysis in [4]. Last but not least, all the case studies in this manuscript are new and they cover a much wider range of events and analysis compared to the conference version in [4].

II. Modal Analysis of Captured Transient Synchronized Waveform Measurements

The starting point in our proposed methodology is to characterize the *transient component* of the synchronized waveform

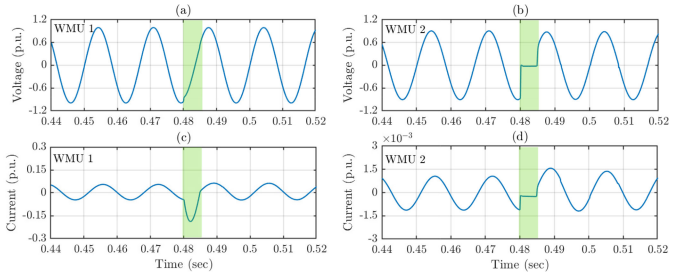

Fig. 2. Synchronized waveform measurements during an incipient fault: (a)-(c) voltage and current waveforms that are captured by WMU 1; (b)-(d) voltage and current waveforms that are captured by WMU 2. The green rectangle marks the transient component that was the subject of modal analysis.

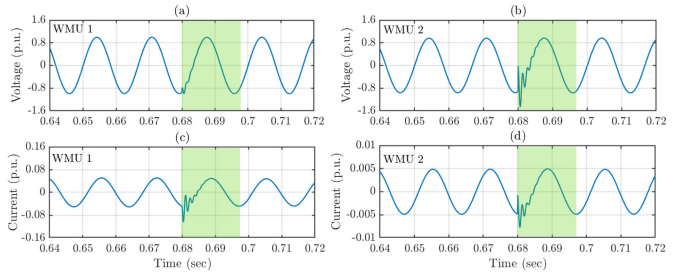

Fig. 3. Synchronized waveform measurements during a capacitor switching: (a)-(c) voltage and current waveforms that are captured by WMU 1; (b)-(d) voltage and current waveforms that are captured by WMU 2. The green rectangle marks the transient component that was the subject of modal analysis.

measurements during an event. Here, we assume that the event *is already detected and classified*, by using any event detection and classification methods, such as those in [2], [5], [26]–[28].

Figs. 2 and 3 show two examples of WMU measurements that are captured during two different types of transient events. The transient components are marked with green boxes. The event in Fig. 2 is an *incipient fault*; it is the same event that we saw in Fig. 1, but this time we also show the voltage waveforms. The event in Fig. 3 is a *capacitor bank switching*. In both events, the duration of the transient part is *one cycle or less*.

We propose to characterize the transient component of the event waveforms by conducting *modal analysis*. In this regard, the transient component of the waveforms is characterized as one or more *oscillation modes*. Each oscillation mode itself is characterized based on the following parameters:

- Frequency,
- Damping Rate,
- Magnitude,
- Phase Angle.

Modal analysis can be done in different ways, such as by using the Prony method [29], matrix pencil method [30], or the methods based on rotational invariance techniques [31].

A. Single-Signal vs Multi-Signal Modal Analysis

Regardless of which method is used, modal analysis can be done in two different ways: *single-signal* and *multi-signal*. There is a considerable difference between these two approaches in the context of this paper, as we explain next.

TABLE I
DOMINANT MODE OF THE TRANSIENT EVENT IN FIG. 2, OBTAINED BY USING THE MULTI-SIGNAL MODAL ANALYSIS

WMU	Signal	Frequency (Hz)	Damping Rate (Hz)	Magnitude (p.u.)	Phase Angle (deg.)
1	Voltage	60.00	0.00	0.96	0.00
	Current			0.32	-35.56
2	Voltage			~ 0.00	-17.94
	Current			~ 0.00	-32.94

TABLE II
DOMINANT MODES OF THE TRANSIENT EVENT IN FIG. 3, OBTAINED BY USING THE MULTI-SIGNAL MODAL ANALYSIS

WMU	Signal	Frequency (Hz)	Damping Rate (Hz)	Magnitude (p.u.)	Phase Angle (deg.)
1	Voltage	60.00 / 747.72	0.00 / -624.30	0.98 / 0.20	0.00 / 0.00
	Current			0.04 / 0.06	-25.19 / 82.43
2	Voltage			0.96 / 0.92	-0.49 / -1.07
	Current			0.004 / 0.004	-25.96 / -3.23

* The two most dominant modes are separated with a slash.

In *single-signal* modal analysis, each individual waveform is analyzed *independently*; thus, the modes are calculated for each waveform *separately*. For instance, for the cases in Figs. 2 and 3, where we have two WMUs, we need to do a separate modal analysis for each of the following four signals within the marked green boxes: voltage waveform at WMU 1, current waveform at WMU 1, voltage waveform at WMU 2, and current waveform at WMU 2. In theory, the frequency should be the same for all the four signals and the damping rate should also be the same for all the four signals; because waveform signals, regardless of where on the circuit they are captured, oscillate at the same frequency and the same damping rate [32].

However, in practice, the results are often slightly different for each signal. This is due to numerical issues, noise in measurements, slight waveform distortions, etc. For example, the fundamental frequency can be obtained as 60.3 Hz from one waveform and 59.9 Hz from another waveform. Such discrepancy can be problematic for the purpose of event location identification that we will discuss in Section III.

The above issue can be resolved by using *multi-signal* modal analysis. In this approach, the transient modes are obtained for all waveforms in the same unified estimation analysis. Hence, the frequency is the same for all the four signals. Likewise, the damping rate is the same for all the four signals.

The dominant mode of the incipient fault in Fig. 2 is shown in Table I. The dominant modes of the capacitor bank switching event in Fig. 3 are shown in Table II. The results in Tables I and II are obtained by using the multi-signal Prony method.

In Tables I and II, the frequency of the dominant mode(s) is the same for all the four waveform signals; and similarly the damping rate of the dominant mode(s) is the same for all the four waveform signals. The reference for the phase angles is with respect to phase angle of the voltage waveform at WMU 1. Also, notice that, the modal analysis in Table I includes one dominant mode while the modal analysis

in Table II includes two dominant modes. Next, we discuss the reason for this key difference between the two types of transient events.

B. Selecting the Time Window and the Number of Modes

There are two basic parameters in any modal analysis: the time window and the number of the modes. The choices of these parameters and their required accuracy depend on the type and the duration of the event. For example, the temporary event in Fig. 2 has a short duration; therefore, it requires a small window size. As another example, the permanent event in Fig. 3 has a much longer duration; therefore, it requires a longer window size; and it is less sensitive to the exact size of the time window for the purpose of the modal analysis. In this paper, we obtain the start time of an event by using the event detection method in [5]; which is proven to accurately obtain the event start time. The method in [5] also provides us with the end time for an event; although, obtaining the end time of an event is usually more challenging. The window size for the purpose of the modal analysis should be equal or less than the time period between the start time and the end time of the event. For example, if we apply the method in [5] on the waveforms in Fig. 2, the start time of the event is obtained at $t = 480$ msec, and the end time of the event is obtained at $t = 485$ msec. Therefore, time window for modal analysis is set to $485 - 480 = 5$ msec or less, see the lengths of the green rectangles in Fig. 2; to make sure that we do not include the part of the signal that is not related to the event.

In this study, we also use an exhaustive search to further refine the window size and also to select the number of modes in the multi-signal modal analysis. For each event, we seek to select these two parameters such that we minimize the *root mean square error* (RMSE) in modal analysis. This is done by conducting the modal analysis for different time windows that are less than the initial time window that we obtain from [5] and also for different number of modes. The RMSE is obtained in each case; and the minimum RMSE is identified and the time window and the number of modes are set accordingly.

C. Selecting the Dominant Transient Event Mode(s)

Depending on the nature of the transient event, it may only magnify an *existing mode*; or it may create *new modes*. The former occurred in the case of the incipient fault in Fig. 2. The latter occurred in the case of the capacitor switching in Fig. 3.

The incipient fault in Fig. 2 was due to a momentary arcing in the system. The arc added a new resistance to the circuit; therefore, it did *not* create any new dynamic mode. As a result, the only dominant mode during the transient event in Fig. 2 is the fundamental mode, i.e., at 60 Hz, as we saw in Table I.

The situation was different for the capacitor bank switching event in Fig. 3. In this case, the event caused a change in the dynamic components of the system; therefore, it created a new dynamic mode of oscillation. As a result, we captured two dominant modes during this transient event. One is the fundamental mode, i.e., at 60 Hz, and the other one is a high-frequency mode, at 748 Hz, as we saw in Table II.

We can use *mode reduction* to decide which dominant mode(s) should be kept for the purpose of our event analysis in Section III. One Option is to keep the modes with high magnitude. Another option is to check the energy of each mode, and keep the modes with high energy.

D. Comparison With Time Domain Analysis

It is insightful to compare some key aspects of our analysis, which is done in modal phasor domain, versus an analysis that could be done in time domain by using the raw waveform measurements. First, the phasor analysis in this paper allows us to focus on the dominant event mode of the signals; which makes our analysis more robust to noises, compared to conducting the analysis on the raw time-series of the waveform measurements. Second, the phasor representation is easier to work with when it comes to solving the circuit. Note that, our method requires conducting the forward analysis and the backward analysis on the circuit model of the underlying power distribution feeder. If we use time representations; then we would have to deal with solving several differential equations and we would have to also consider an *initial solution*; all of which would unnecessarily complicate the analysis. Third, we use phasor representation only for the exact duration of the event, which ranges from less than a cycle to a few cycles. Thus, we inherently focus on the specific short interval of the *transient* component of the event. Fourth, the proposed method uses the Prony method to capture the dominant event modes in the waveform signals, as opposed to using the fast Fourier transformation. Therefore, although our analysis is done in phasor domain, we do *not* lose the information about the event, unlike in the case of the phasor measurements in PMUs. In fact, we fully capture the transient behavior of the event, even if it is only a short period of time.

III. Constructing the Feeder Model at the Dominant Transient Modes

Given the dominant modes of the synchronized waveform measurements during the transient event, the next step is to construct the feeder circuit model at those dominant modes. In this regard, consider the power distribution feeder that we saw in Fig. 1(a), and let us focus on any arbitrary line segment in this feeder, such as the one that is shown in Fig. 4(a). Let R and L denote the resistance and inductance of the line segment.

Suppose a transient event occurs at time $t = 0$ at a bus on the distribution feeder. Suppose the location of the event is *unknown*. The voltage waveform at bus m is denoted by $v_m(t)$; the voltage waveform at bus n is denoted by $v_n(t)$; and the current waveform on the line segment is denoted by $i_m(t)$, where t indicates the timestamp immediately after the event.

As mentioned in Section II-C, the transient event may either only magnify the existing fundamental mode; or it may create new dominant modes. Next, we discuss how to model the circuit of the distribution feeder under both circumstances.

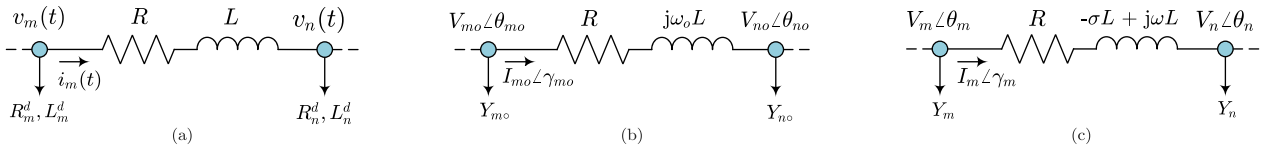

Fig. 4. Analysis of voltage and current waveforms at a line segment immediately after the transient event occurs: (a) the circuit model in time domain; (b) the circuit model under the *fundamental mode*; (c) the circuit model under the *new transient mode* that might be created by the event.

A. Case I: Transient Event Does Not Create a New Mode

If the transient event does *not* create any new oscillation mode, e.g., as in Fig. 2, then the only dominant mode during the transient event is the fundamental mode, as in Table I.

Let $f_\circ$ and $\omega_\circ = 2\pi f_\circ$ denote the frequency and rotational frequency of the fundamental mode. Also, let $V_{m\circ}$ and $\theta_{m\circ}$ denote the magnitude and phase angle of $v_m(t)$ at the fundamental mode; $V_{n\circ}$ and $\theta_{n\circ}$ denote the magnitude and phase angle of $v_n(t)$ at the fundamental mode; and $I_{m\circ}$ and $\gamma_{m\circ}$ denote the magnitude and phase angle of $i_m(t)$ at the fundamental mode. We can write the voltage difference between buses m and n at the fundamental mode as follows:

$$V_{m\circ}\angle\theta_{m\circ} - V_{n\circ}\angle\theta_{n\circ} = Z_\circ I_{m\circ}\angle\gamma_{m\circ}, \tag{1}$$

where

$$Z_\circ = R + \mathrm{j}\omega_\circ L \tag{2}$$

is the impedance of the line at the fundamental mode. The circuit model under the fundamental mode is as in Fig. 4(b).

B. Case II: Transient Event Creates a New Mode

If the transient event creates a new oscillation mode, e.g., as in Fig. 3, then the dominant modes are not only the fundamental mode but also one or more new modes, as in Table II. Without loss of generality, we assume that there exists only one new dominant mode in the transient event. If the transient event introduces multiple new modes, then we can simply take the dominant mode and the rest of the analysis remains the same.

Let f, $\omega = 2\pi f$, and $-\sigma$ denote the frequency, the rotational frequency, and the damping rate of the new event mode. Also, let V_m and θ_m denote the magnitude and phase angle of $v_m(t)$ at the new event mode; V_n and θ_n denote the magnitude and phase angle of $v_n(t)$ at the new event mode; and I_m and γ_m denote the magnitude and phase angle of $i_m(t)$ at the new event mode. We write the voltage difference between buses m and n at the new event mode as follows:

$$V_m\angle\theta_m - V_n\angle\theta_n = ZI_m\angle\gamma_m, \tag{3}$$

where

$$Z = R - \sigma L + \mathrm{j}\omega L \tag{4}$$

is the impedance of the line at the new event mode. The circuit model under the new event mode is shown in Fig. 4(c). Notice the difference between (2) and (4) and the fact that the damping rate of the new event mode appears as a *resistive* term in (4).

C. Load Modeling in Cases I and II

We assume that the active and reactive power loads are given at all buses, either by direct measurements, such as via smart meters; or by using pseudo-measurements, such as via historical data or the ratings of the load transformers. This is a reasonable assumption; because the rating of the load transformers and the substation measurements are always available in practice. Importantly, the proposed method is very robust against errors in pseudo-measurements; as we will verify through case studies in Section V-G2. Thus, we can estimate the equivalent resistance and inductance of the load at each bus. Let R_m^d and L_m^d denote the resistance and inductance of the load at bus m; and R_n^d and L_n^d denote the resistance and inductance of the load at bus n, as we already marked in Fig. 4(a). We can express the admittance of the loads at buses m and n at the fundamental mode in Case I in Section III-A as:

$$\begin{aligned} Y_{m\circ} &= 1/\left(R_m^d + \mathrm{j}\omega_\circ L_m^d\right), \\ Y_{n\circ} &= 1/\left(R_n^d + \mathrm{j}\omega_\circ L_n^d\right). \end{aligned} \tag{5}$$

Similarly, we can express the admittance of the loads at buses m and n at the new event mode in Case II in Section III-B as:

$$\begin{aligned} Y_m &= 1/\left(R_m^d - \sigma L_m^d + \mathrm{j}\omega L_m^d\right), \\ Y_n &= 1/\left(R_n^d - \sigma L_n^d + \mathrm{j}\omega L_n^d\right). \end{aligned} \tag{6}$$

Notice the difference between (5) and (6). The damping rate of the new event mode appears as a *resistive* term in (6).

In (5) and (6), we assume that all loads are constant impedance. However, other types of loads, namely constant current and constant power loads, can also be similarly formulated and integrated into the model using pseudo-measurements. The use of other types of loads is discussed in Appendix B.

IV. Event Location Identification Method

In this section, we propose a method to pin-point the location of a transient event. We assume that the synchronized waveform measurements are already characterized by their multi-signal modal analysis, as in Section II; and the distribution feeder is already modeled, as in Section III-A or Section III-B, depending on whether the transient event magnifies the existing fundamental mode or it creates a new event mode, respectively.

A. Methodology

Consider a power distribution feeder that has N buses, as in Fig. 1(a). Suppose two WMUs are installed on the distribution

feeder, one at the beginning of the feeder at bus 1 and one at the end of the feeder at bus N. Suppose a transient event occurs somewhere along the feeder at *unknown* bus $k \in \{1, \ldots, N\}$.

1) Forward Sweep and Backward Sweep: The starting point in our event location identification method is to conduct a forward sweep and a backward sweep, see [33, Ch. 10], on the constructed circuit model of the distribution feeder.

In forward sweep, we start from the phasor representation of the *dominant mode* that is obtained in WMU 1 at bus 1, and we calculate the nodal voltages at all the buses on the distribution feeder at the dominant mode, all the way forward to WMU 2 at bus N. We denote the results in forward sweep by

$$V_1^f, \ldots, V_{k-1}^f, V_k^f, V_{k+1}^f, \ldots, V_N^f. \tag{7}$$

In backward sweep, we start from the phasor representation of the *dominant mode* that is obtained in WMU 2 at bus N, and we calculate the nodal voltages at all the buses on the distribution feeder at the dominant mode, all the way back to WMU 1 at bus 1. We denote the results in backward sweep by

$$V_1^b, \ldots, V_{k-1}^b, V_k^b, V_{k+1}^b, \ldots, V_N^b. \tag{8}$$

Note that, if the transient event does *not* create any new mode, then we use the line impedance in (2) and the load admittance in (5) to conduct forward sweep and backward sweep. However, if the transient event *does* create any new mode, then we use the line impedance in (4) and the load admittance in (6) to conduct forward sweep and backward sweep.

2) Minimizing Discrepancy: Let Ψ_i denotes the *discrepancy index* at bus i between the results from the forward sweep in (7) and the results from the backward sweep in (8):

$$\Psi_i = |V_i^f - V_i^b|, \ \forall\, i = 1, \ldots, N, \tag{9}$$

where $|.|$ returns the magnitude of a complex number. The location of the transient event is obtained as follows:

$$k^\star = \arg\min_i \Psi_i. \tag{10}$$

The basic idea in (10) comes from the analysis in [10] that was developed for PMU measurements. Here, we extend the idea to the case where the phasors in forward sweep and backward sweep are based on the dominant mode of the transient event that is obtained by doing a multi-signal modal analysis across all the synchronized waveform measurements at WMU 1 and WMU 2. The rational in (10) is that the forward sweep and the backward sweep both start from direct measurements at a WMU and they continue to be correct up until we pass the unknown event bus k. At that point, the results of forward sweep and backward sweep both become incorrect. In the forward sweep, $V_1^f, \ldots, V_k^f$ are calculated correctly; while $V_{k+1}^f, \ldots, V_N^f$ are calculated incorrectly. In the backward sweep, $V_1^b, \ldots, V_{k-1}^b$ are calculated incorrectly; while $V_k^b, \ldots, V_N^b$ are calculated correctly. We can conclude that $V_i^f = V_i^b$ for $i = k$, while $V_i^f \neq V_i^b$ for $i \neq k$. Thus, the location of the transient event is obtained as in (10).

Algorithm 1 Event Location Identification: Two WMUs

Input: WMU measurements and network data
Output: The location of the transient event

// Step I:
Use multi-signal modal analysis to obtain the dominant mode(s) of the captured waveforms during the transient event, such as within the green boxes in Figs. 2 and 3.
// Step II:
if the event does not create a new mode **then**
  Construct the circuit model based on (1), (2), and (5).
else if the event creates a new mode **then**
  Construct the circuit model based on (3), (4), and (6).
end if
// Step III:
Use forward sweep to obtain the nodal voltages in (7).
Use backward sweep to obtain the nodal voltages in (8).
Calculate the voltage discrepancies as in (9).
Obtain the event bus number by using (10).

Algorithm 2 Event Location Identification: Multiple WMUs

Input: WMU measurements and network data
Output: The location of the transient event

for the WMU at each bus $s \in \Omega\backslash\{1\}$ **do**
  Use Algorithm 1 to obtain $\Psi_i^{1,s}$ at each bus i.
end for
Obtain Ψ_i at each bus i using (11).
Obtain the event bus number using (10).

B. Algorithm

By combining the analysis in Sections II, III, and IV-A, we can develop a three-step algorithm to identify the location of transient events by using synchronized WMU measurements, as shown in Algorithm 1. In Step I, we extract the characteristics of the transient event from the captured synchronized waveform measurements by doing a multi-signal modal analysis. In Step II, we construct the circuit model of the feeder under the dominant mode(s). In Step III, we conduct a forward sweep and a backward sweep on the constructed circuit model, followed by the discrepancy analysis to identify the location of the event.

C. Extension to Arbitrary Number of WMUs

Suppose multiple WMUs are available, one is at the beginning of the feeder, and the rest are at the end of the feeder/laterals, as in Fig. 5. Suppose Ω is the set of buses with WMUs. For the WMU at each bus $s \in \Omega\backslash\{1\}$, let us define $\Psi_i^{1,s}$ as the discrepancy index at bus i that is obtained by using (9); where we start the forward sweep from the WMU at bus 1 and we start the backward sweep from the WMU at bus s. We define

$$\Psi_i = \sum_{s \in \Omega\backslash\{1\}} \Psi_i^{1,s}, \ \forall\, i = 1, \ldots, N. \tag{11}$$

Accordingly, we identify the location of the transient event at the minimum of the above combined discrepancy index. The exact procedure is shown in Algorithm 2.

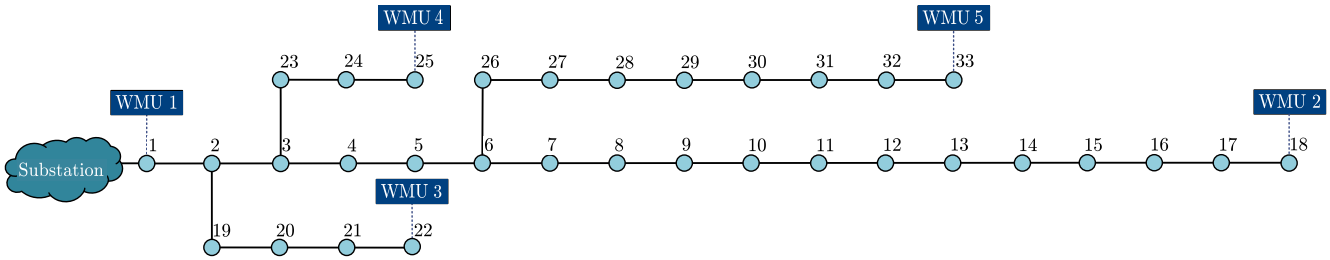

Fig. 5. The IEEE 33-bus distribution system with five WMUs, where the set of buses with WMUs is $\Omega = \{1, 18, 22, 25, 33\}$.

V. Case Studies

In this section, we assess the performance of the proposed event location identification method by applying it to the IEEE 33-bus test system. The single line diagram of the test system is shown in Fig. 5. Five WMUs are installed on this network; as marked on the figure. Each WMU reports the synchronized voltage and current waveform measurements. The waveform measurements in this study are taken from the PSCAD/EMTDC simulation [34] and supplied to the event location identification algorithm. The nominal frequency of the system is 60 Hz. Unless stated otherwise, the reporting rate of the WMUs is assumed to be 256 samples per cycle. The incipient fault is simulated in form an arc based on the existing Cassie model in PSCAD [35], [36]. We study different scenarios of transient events, such as sub-cycle incipient faults and multi-cycle incipient faults, and permanent events, such as permanent faults and capacitor bank switching events.

A. Scenario I: Sub-Cycle Incipient Fault

Suppose a sub-cycle incipient fault occurs at bus 9 and it lasts for *one quarter of a cycle*. Fig. 2 in Section II shows the voltage and current waveforms during this event that are captured by WMUs 1 and 2. First, we extract the modes of all the 10 waveforms from all the five WMUs by conducting a multi-signal modal analysis. The results for WMUs 1 and 2 are already shown in Table I. Recall that this event does *not* create any new mode. Next, we construct the circuit model between the WMU at bus 1 and any of the other four WMUs at buses 18, 22, 25, and 33. Finally, we run Algorithm 1 for each pair of WMUs; or we run Algorithm 2 for all five WMUs.

The results of running Algorithm 1 are shown in Figs. 6(a)–(d); and the results of running Algorithm 2 are shown in Fig. 6(e). As shown in Fig. 6(a), if the waveform measurements are available only from WMUs 1 and 5, then the discrepancy index is minimized at buses 6 to 18, indicating that the incipient fault occurred somewhere at the downstream of bus 6. As shown in Fig. 6(b), if the waveform measurements are available only from WMUs 1 and 4, then the discrepancy index is minimized at buses 3 to 18, and buses 26 to 33, indicating that the fault occurred at one of these buses. As shown in Fig. 6(c), if the waveform measurements are available only from WMUs 1 and 3, then the discrepancy index is minimized at buses 2 to 18, and buses 23 to 33, indicating that the fault occurred at one of these buses. As shown in Fig. 6(d), if the waveform measurements are available only from WMUs 1 and 2, then the discrepancy index is minimized at bus 9; which is the correct event bus. Finally, as shown in Fig. 6(e), if the waveform measurements are available from all the five WMUs, the minimum discrepancy index occurs at bus 9; which is the correct event bus.

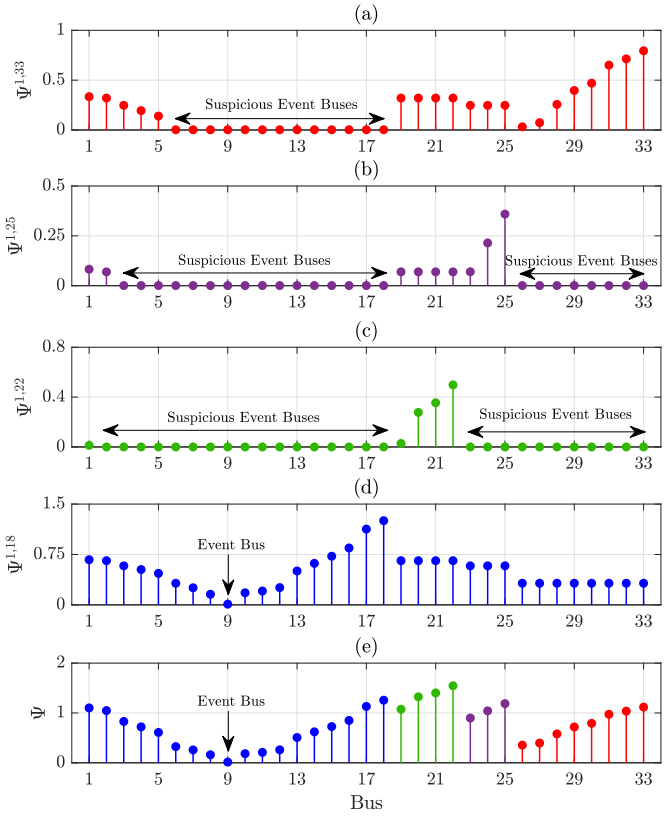

Fig. 6. Discrepancy index in Scenario I, when the sub-cycle incipient fault occurs at bus 9 using the measurements from: (a) WMUs 1 and 5; (b) WMUs 1 and 4; (c) WMUs 1 and 3; (d) WMUs 1 and 2; (e) WMUs 1 to 5.

From the above cases, we can conclude that the proposed method is able to identify the correct location of the event even if *only two* WMUs are available; as long as the event occurs somewhere *between* those two WMUs. For example, suppose only WMU 1 and WMU 2 are available. In that case, we can *correctly* identify the location of the event if the event occurs anywhere on the main feeder, i.e., at buses 1, 2, 3, ..., 17, or 18. However, if the event occurs somewhere on the *first* lateral, i.e., at buses 19, 20, 21, or 22, then we identify bus 2, i.e., the head of the first lateral, as the event bus. This is because we do *not* have any WMU on the first lateral; of course, unless we *do* install WMU 3 at bus 22; which in that

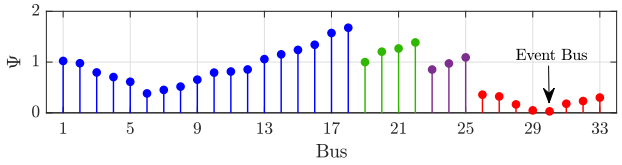

Fig. 7. Discrepancy index in Scenario II, when the multi-cycle incipient fault occurs at bus 30, based on running Algorithm 2 on all five WMUs.

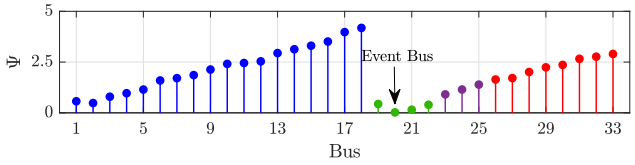

Fig. 8. Discrepancy index in Scenario III, when the permanent fault occurs at bus 20, based on running Algorithm 2 on all five WMUs.

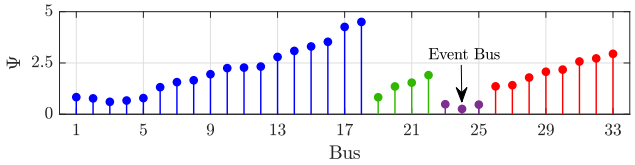

Fig. 9. Discrepancy index in Scenario IV, when capacitor bank switching occurs at bus 24, based on running Algorithm 2 on all five WMUs.

case we *can* identify the exact location of the event on the first lateral. Similarly, if the event occurs somewhere on the *second* lateral, i.e., at buses 23, 24, or 25, then we identify bus 3, i.e., the head of the second lateral, as the event bus. This is because we do *not* have any WMU on the second lateral; of course, unless we *do* install WMU 4 at bus 25; which in that case we *can* identify the exact location of the event on the second lateral. Similarly, if the event occurs somewhere on the *third* lateral, i.e., at buses 26, 27, ..., 32 or 33, then we identify bus 6, i.e., the head of the third lateral, as the event bus. This is because we do *not* have any WMU on the third lateral; of course, unless we *do* install WMU 5 at bus 33; which in that case we *can* identify the exact location of the event on the third lateral. In summary, the proposed method can work with at least two WMUs; depending on the location of the transient event, certain pairs of WMUs are more suitable to provide the waveform measurements that can lead to correctly identify the location of the event by running Algorithm 1. However, since the event bus is *not* known in advance, it is necessary that we use the waveform measurements from all the five WMUs so that we can identify the exact location of the event; whether it occurs on the main feeder or on a lateral. For the rest of this paper, we focus on identifying the event bus using the waveform measurements from all the five WMUs.

B. Scenario II: Multi-Cycle Incipient Fault

Suppose a multi-cycle incipient fault occurs at bus 30 and it lasts for *two cycles*. As in Scenario I, this event does *not* create any new mode. Fig. 7 shows the results of running Algorithm 2 in this scenario based on the waveform measurements from all five WMUs. As we can see, our method is able to correctly identify bus 30 as the location of the incipient fault. This scenario further confirms the accuracy of our method.

C. Scenario III: Permanent Fault

Suppose a permanent symmetric fault occurs at bus 20. We call it permanent because it is *not* self-cleared. It may last until it is cleared by a circuit breaker. As in Scenarios I and II; this permanent fault does *not* create any new mode. The results of running Algorithm 2 are shown in Fig. 8. The location of the permanent fault is correctly identified at bus 20. The results in this scenario confirm the accuracy of the proposed method even for transient events that lead to permanent events. Of course, our method still focuses only on the transient component of this event; and accordingly, it identifies its location very promptly. We will examine the performance of the proposed method for asymmetric faults in unbalanced networks later in Section V-I.

D. Scenario IV: Capacitor Bank Switching Event

Suppose a capacitor bank is switched on at bus 24. Fig. 3 in Section II shows the voltage and current waveforms during this event that are captured by WMUs 1 and 4. The results of multi-signal modal analysis are already shown in Table II. Unlike in Scenarios I, II, and III, in this scenario, the event not only magnifies the fundamental mode but it also creates a new dominant mode, as we saw in Table II. The results of running Algorithm 2 are shown in Fig. 9. As we can see, the proposed method is able to identify the correct event location.

E. Impact of Measurement Reporting Rate

Different types of WMUs may have different reporting rates. A higher reporting rate results in more information about the system and the event, but it requires larger data storage capabilities and faster data communication. A lower reporting rate leads to less information about the event, but it requires less computational efforts. Therefore, the reporting rate of WMUs can play an important role in the performance of any data-driven event analysis. In this regard, we examine the performance of the proposed event location identification method by down-sampling the reporting rate from 256 samples per cycle to 128, 64, and 32 samples per cycle. The results reveal that even when the reporting rate is as low as only 32 samples per cycle, the proposed method is able to correctly identify the location of the events in all the four types of events that we had discussed in Sections V-A–V-D.

F. Performance Comparison

In this section, we compare the performance of our method with that of two state-of-the-art methods in [11] and [24].

1) Multi-Cycle Incipient Fault: In [11]; a distance-based method is proposed to identify the location of incipient faults. This method uses the waveform measurements from WMU 1 to estimate the distance between the fault location and the sensor location. This method does not use the measurements from the rest of the WMUs; because the fault current almost entirely flows through the substation and not through the loads. Figs. 10(a) and (b) show the estimated resistance and reactance, respectively, for the case of the multi-cycle incipient

TABLE III
COMPARISON BETWEEN [11], [24], AND THE PROPOSED METHOD

	[11]	[24]	Proposed Method
Methodology	Impedance-based	Initial Value-based	Wide Area-based
Type of Events	Faults	Capacitor Switching	Both
Use of Time Synchronization	No	No	Yes
Location Identification Accuracy	Low	Low	High
Robust Against Intermediate Loads	No	No	Yes

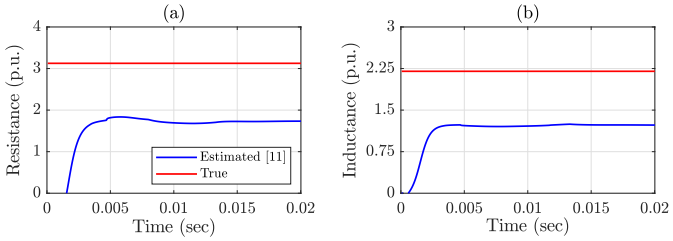

Fig. 10. The results of estimating the impedance of an incipient fault by using the impedance-based method in [11]: (a) the estimated resistance; (b) the estimated inductance.

fault in Scenario II in Section V. As we can see, the estimated impedance does not converge to the correct values. This is because there are loads between the sensor location and the fault location. They result in underestimating the impedance. This issue is alleviated by approximating the loads based on the measurements before the event occurs [21]. Translating the estimated impedance to distance and then to bus number, one can identify bus 27 as the event bus; which is *incorrect*. It is three buses away from bus 30, which is the correct bus. This method also identifies bus 7 as the event bus. This is of course the main drawback of impedance-based methods that identify *multiple* locations for the event, see [14]. In summary, the method in [11] cannot identify the correct event bus. However, as we already saw in Fig. 7, our method can correctly identify the location of the incipient fault at bus 30.

2) Capacitor Bank Switching: In [24], a method is proposed to identify the location of the capacitor bank switching event. The method is based on the Initial Value Theorem in circuit theory. It estimates the distance between the sensor location and the capacitor bank location by using the instantaneous voltages *before* and *after* the event. If we apply the method in [24] to the capacitor bank switching event in Scenario IV in Section V, we can obtain the pre-event instantaneous voltage and the post-event instantaneous voltage as $v(t^-) = -0.952$ p.u. and $v(t^+) = -0.777$ p.u. According to [24], we can estimate the inductance from the sensor location to the event location as

$$L^{\text{est}} = \frac{v(t^+)}{v(t^-) - v(t^+)} L^{\text{th}}, \tag{12}$$

where L^{th} is the Thevenin inductance seen by WMU 1.

The estimated inductance is obtained as 1.049 p.u.; however the true inductance is 2.276 p.u. Translating this estimation to bus number, we identify bus 23 as the event bus. However, this is not the correct event bus. It is rather the neighboring bus of the correct bus, i.e., bus 24. It should be noted that the estimated inductance is smaller than the true one. This is because there are loads between the sensor location and the fault location, which affect the estimation of impedance. In summary, the method in [24] is not able to identify the correct event bus. However, as we already saw in Fig. 9, our proposed method is able to correctly identify the location of the capacitor bank at bus 24.

Table III summarizes the comparison between the methods in [11], [24] and the proposed method. First, the method in [11] is designed to locate only faults, which are very severe events; and the method in [24] is designed to locate only capacitor bank switching events; however, the proposed method in this paper can locate both types of events. Second, the proposed method is specifically designed to take advantage of the *synchronized measurements* from *multiple* WMUs; as opposed to the methods in [11] and [24] that inherently work based on measurements from one sensor; because they were designed before the advent of WMUs which have emerged only very recently. Third, the proposed method is able to identify the location of events with higher accuracy, as opposed to the methods in [11] and [24] that identify the location of certain events with considerable error. Fourth, the proposed method is not sensitive to the intermediate loads between the event location and the sensor location; as we will see in Section V-G3. However, such robustness is not reported for the methods in [11] and [24].

It bears mentioning that we absolutely do *not* say that there is any problem with the existing methods that use measurements from only one power quality sensor (which is the ancestor of WMU). Instead, we make the following argument: now that synchronized waveform measurements from *multiple* WMUs are gradually becoming available in practice, let us design methods that can take advantage of such *synchronized waveform* availability. The proposed method in this paper tries to exactly do so by proposing a method that *does* take advantage of having access to synchronized waveform measurements from *multiple* WMUs. Furthermore, we show that once such data availability from multiple WMUs is used, the results can outperform the traditional methods that are designed to use waveform measurements from only one power quality sensor.

G. Sensitivity Analysis

Next, we use Monte Carlo simulation to assess the impact of errors in parameters and measurements on the accuracy of the proposed method. The number of random scenarios is 10,000.

1) Error in Line Parameters: Line inductance and resistance may deviate from their nominal values because of loading, aging, and weather conditions, to name a few. Table IV

TABLE IV
IMPACT OF ERROR IN LINE PARAMETERS

Error (%)	Correct Bus	Neighboring Bus	Other Bus
25	100.0 %	0.0 %	0.0 %
50	98.9 %	1.1 %	0.0 %
75	93.0 %	7.0 %	0.0 %
100	85.8%	14.2 %	0.0 %

TABLE V
IMPACT OF ERROR IN PSEUDO-MEASUREMENTS

Error (%)	Correct Bus	Neighboring Bus	Other Bus
25	100.0 %	0.0 %	0.0 %
50	100.0 %	0.0 %	0.0 %
75	100.0 %	0.0 %	0.0 %
100	99.8 %	0.1 %	0.1 %

TABLE VI
IMPACT OF HARMONIC DISTORTION AND MEASUREMENT NOISE ON THE ACCURACY OF THE EVENT LOCATION IDENTIFICATION METHOD

THD (%)	SNR (dB)	Correct Bus	Neighboring Bus	Other Bus
1	80	100.0 %	0.0 %	0.0 %
	50	100.0 %	0.0 %	0.0 %
	20	86.8 %	5.8 %	7.4 %
2	80	100.0 %	0.0 %	0.0 %
	50	99.9 %	0.1 %	0.0 %
	20	84.4 %	7.5 %	8.1 %
3	80	100.0 %	0.0 %	0.0 %
	50	99.8 %	0.2 %	0.0 %
	20	85.5 %	6.2 %	8.3 %

shows the results for different levels of errors. As we can see, even when the error is at 50%, the proposed method can identify the correct location for the transient event in 98.9% of the random scenarios. In the remaining 1.1% of the cases, we identify the neighboring bus as the event location. Hence, the robustness of the proposed method is confirmed for errors in line parameters.

2) Error in Pseudo-Measurements: Table V shows the location identification accuracy for different levels of errors in pseudo-measurements. Even when the error is at 100%, the proposed method can identify the correct location for the transient even in 99.8% of the random scenarios. In another 0.2% of the cases, we can still identify the neighboring bus. Thus, the robustness of the proposed method is further confirmed.

3) Noise and Harmonics in Waveform Measurements: Table VI shows the results on the accuracy of the proposed event identification method for different levels of harmonics in the system as well as different levels of measurement noise in WMU measurements. The level of harmonics is specified in terms of the *total-harmonic-distortion* (THD) of the current waveforms. The measurement noise level is specified in terms of the *signal-to-noise-ratio* (SNR). As we can see, even when the THD is as high as 3% and the SNR is as low as 20 dB, the proposed method is still able to correctly identify the location of the event in 85.5% of the random scenarios. In another 6.2% of the random scenarios, an immediate neighboring bus of the correct event bus is identified. The results in Table VI confirm the robustness of the proposed event location identification method even under considerable harmonic and measurement noise levels. It bears mentioning that,

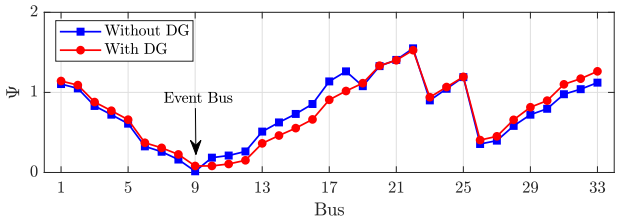

Fig. 11. Comparing the discrepancy indices in identifying the location of the sub-cycle incipient fault in Scenario I in an *active* network and a *passive* network by running Algorithm 2 on all five WMUs.

identifying the correct location of sub-cycle incipient faults becomes challenging when the levels of noise and harmonics in waveform measurements are high, due to the very short duration of such events.

H. Active Distribution Networks

In this section, we apply the proposed method on an active power distribution network, i.e., a power distribution system with a Distributed Generation (DG) unit. In this regard, we install a DG at bus 33. Importantly, we do *not* include any knowledge about this DG in our analysis. In other words, we assume that we are *unaware* of the presence of this DG. Fig. 11 shows the results of running Algorithm 2 for the case of the sub-cycle incipient fault in Scenario I in Section V-A, when the DG *is* connected to the network and when it is *not* connected to the network. As we can see, the proposed method is still able to correctly identify the location of the incipient fault at bus 9, even in the presence of the DG. Notice that, when the DG is connected to the network, the difference between the lowest discrepancy index and the second lowest discrepancy index is smaller; this means that the event location identification is now more challenging. However, this is simply because we assume that we do *not* know about the presence of the DG in Algorithm 2; yet we are still able to identify the location of the event correctly. If we *do* know the about the DG, i.e., its location and its size, then we can reach the same original accuracy as in the case when the DG is not connected to the network.

I. Extension to Unbalanced Three-Phase Networks

In this section, we apply the proposed event location identification method to an unbalanced three-phase power distribution network with asymmetric events. In this regard, first, we extend the IEEE 33-bus test system to an unbalanced three-phase network by changing the loading on the three phases. Other parameters and assumptions remain the same as those mentioned for the initial test system. Suppose a permanent two-phase line-to-ground fault on Phases A and B occurs at bus 20. It is an asymmetric event. Similar to the case of the fault in Scenario III in Section V-C, this fault does not create any new mode in the system. Fig. 12 shows the results of running Algorithm 2 on Phases A, B, and C. As we can see, the discrepancy index on Phases A and B is minimized at bus 20, indicating that the fault occurred at bus 20, which is correct. However, the discrepancy index on Phase C is almost zero at all buses, correctly indicating that the fault did not occur on

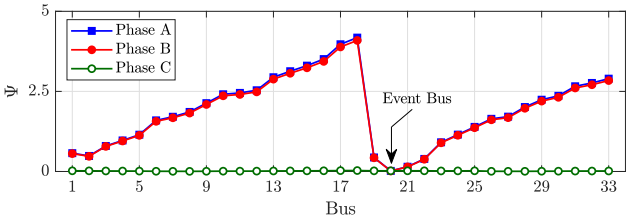

Fig. 12. Discrepancy indices on different phases in identifying the location of an *asymmetric phase-to-phase* fault at bus 20, across Phases A and B, in an *unbalanced three-phase* network by running Algorithm 2 on all five WMUs.

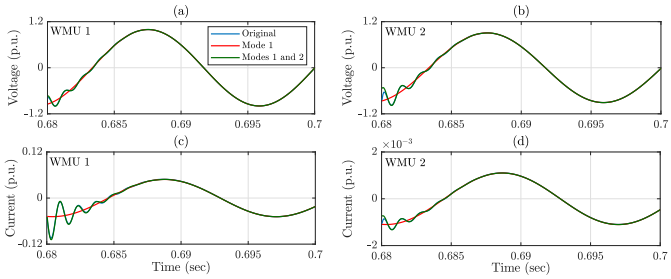

Fig. 13. An example for multi-signal Prony analysis in Appendix A: (a)-(b) voltage signals; (c)-(d) current signals. The blue curves are the original transient component of the waveform measurements in Fig. 3. The red curves are the reconstructed waveform measurements by using the first dominant mode. The green curves are the reconstructed waveform measurements by using both the first and the second dominant modes.

Phase C. It should be noted that, there are small differences between the discrepancy indices on Phase A and Phase B. These differences are due to the load imbalance across the phases. Nevertheless, the proposed method is able to identify the correct bus as the location of the fault and it can also correctly identify Phases A and B as the phases of the fault. We can conclude that the proposed method can work well even for asymmetric events in unbalanced three-phase power distribution networks.

VI. Conclusion

This paper introduced a new application for WMUs, as an emerging smart grid sensor technology; while it also addressed a challenging problem in power distribution systems. In this regard, a novel three-step method is proposed to use synchronized waveform measurements from WMUs to identify the location of transient events, including sub-cycle and multi-cycle incipient faults, in power distribution networks. The proposed method requires installing at least two WMUs, but its performance can further improve if we use multiple WMUs. Unlike the methods that use phasor measurements, which inherently require reaching the steady-state conditions before they can be applied, the proposed method is prompt; because it uses the waveform measurements during the transient conditions of the event. The method was tested on the IEEE 33-bus distribution network for different cases of transient events. The results confirmed the accuracy of the method in identifying the correct location of the transient events; even for very short events. The proposed method can also identify the location of permanent events, such as permanent symmetric and asymmetric faults and capacitor bank switching events. The proposed method is robust against error in line parameters and error in load parameters. The latter is particularly important in practice; because the real-world load parameters can be in form of inaccurate pseudo-measurements. Furthermore, the proposed method can reach a high accuracy, even with noisy waveform measurements and also at low measurement reporting rates. It works well also in active power distribution networks and in unbalanced three-phase networks, making the proposed method applicable in most practical power distribution networks.

Appendix A
Multi-Signal Modal Analysis

The multi-signal modal analysis in this paper is done by using the multi-signal Prony method to simultaneously extract the modes of multiple waveform measurements. This is done by applying optimal curve fitting to the waveform measurements by using the least squares technique. Suppose $x_m(t)$ is one of the signals of the waveform measurements, where $m = 1, \ldots, M$. Here, M is the number of signals. For example, if we have two WMUs and each WMU provides one signal for voltage waveform measurements and one signal for current waveform measurements, then $M = 4$. The goal of the Multi-signal Prony method is to fit a *damped sinusoidal model* to $x_m(t)$, along with all other waveform signals in the system, to estimate $\hat{x}_m(t)$ as follows:

$$\hat{x}_m(t) = \sum_{p=1}^{P} A_{p,m}\, e^{\sigma_p t}\, cos\big(2\pi f_p t + \theta_p\big), \tag{13}$$

where f_p and σ_p denote the frequency and the damping rate at mode p in the system; and $A_{p,m}$ and $\theta_{p,m}$ denote the amplitude and phase angle at mode p of waveform measurement m. Notice that, while f_p and σ_p are the same for all signals, each signal has its own $A_{p,m}$ and $\theta_{p,m}$. In this regard, the phasor representation of waveform signal $x_m(t)$ at mode p is $A_{p,m} \angle\theta_{p,m}$. Fig. 13 shows an illustrative example of the original transient components for each signal $x_m(t)$ of the total of $M = 4$ waveform measurements in Fig. 3, and their corresponding signal estimations $\hat{x}_m(t)$. The *blue* curves are the original waveforms, i.e., $x_m(t)$, the *red* curves are the estimated waveforms, i.e., $\hat{x}_m(t)$, which are obtained by using the first dominant mode, and *green* curves are the estimated waveforms, i.e., $\hat{x}_m(t)$, which are obtained by using the first and the second dominant modes. As we can see, the *reconstructed* waveforms using the first two dominant modes fit the original waveforms the best. The *root mean square error* (RMSE) of the red curves is about 2.4%, and the RMSE of the green curves is about 0.5%. Therefore, we can fully capture the transient behavior of the capacitor bank switching event with only the first two dominant modes. The characteristics of the first two dominant modes are shown in Table II in the main body of the paper.

Appendix B
Load Types

Any load can be expressed in the generic form of an exponential model [37]. Specifically, the apparent power

consumption of the load connected to bus i can be modeled as:

$$S_i = P_{i\circ}\left(\frac{V_i}{V_{i\circ}}\right)^{\eta_p} + Q_{i\circ}\left(\frac{V_i}{V_{i\circ}}\right)^{\eta_q}, \tag{14}$$

where $P_{i\circ}$, $Q_{i\circ}$, and S_i denote the nominal active power, nominal reactive power, and operating apparent power of the load at bus i; $V_{i\circ}$ and V_i denote the nominal and operating nodal voltage of bus i. In (14), if $\eta_p = 0, 1, 2$, then the load is *constant power*, *constant current*, and *constant impedance*, respectively. The reactive power component can be defined similarly by using η_q. In this equation, the nominal values $S_{i\circ}$ and $V_{i\circ}$ are known at each bus i; and the operating nodal voltage V_i is obtained from forward sweep and backward sweep calculations in (7) and (8). As a result, one can obtain S_i from (14) depending on the type of the load. Next, the resistance and inductance of the load at bus i is obtained as follows:

$$R_i^d = \mathrm{Re}\left\{\frac{V_i^2}{S_i^*}\right\},\ L_i^d = \frac{1}{\omega_\circ}\mathrm{Im}\left\{\frac{V_i^2}{S_i^*}\right\} \tag{15}$$

where * returns the complex conjugate; Re{.} and Im{.} return the real part and the imaginary part, respectively. Once the resistance and inductance are obtained, the admittance of the load can be obtained via either (5) or (6), depending on the dominant mode. Of course, this makes the nodal voltages in (7) and (8) more complicated to calculate. However, the rest of the analysis in Section IV, which is based on examining the discrepancy between the forward sweep and backward sweep calculations, will remain the same.

REFERENCES

[1] K. L. Butler-Purry and M. Bagriyanik, "Characterization of transients in transformers using discrete wavelet transforms," *IEEE Trans. Power Syst.*, vol. 18, no. 2, pp. 648–656, May 2003.

[2] T. S. Sidhu and Z. Xu, "Detection of incipient faults in distribution underground cables," *IEEE Trans. Power Del.*, vol. 25, no. 3, pp. 1363–1371, Jul. 2010.

[3] A. F. Bastos, S. Santoso, W. Freitas, and W. Xu, "SynchroWaveform measurement units and applications," in *Proc. IEEE PES Gen. Meeting*, Atlanta, GA, USA, 2019, pp. 1–5.

[4] M. Izadi and H. Mohsenian-Rad, "Event location identification in distribution networks using waveform measurement units," in *Proc. IEEE PES Innovat. Smart Grid Technol. Eur. (ISGT-Europe)*, Hague, The Netherlands, 2020, pp. 924–928.

[5] M. Izadi and H. Mohsenian-Rad, "A synchronized Lissajous-based approach to achieve situational awareness using synchronized waveform measurements," in *Proc. IEEE PES Gen. Meeting*, Washington, DC, USA, 2021, pp. 1–5.

[6] M. Izadi and H. Mohsenian-Rad, "Characterizing synchronized Lissajous curves to scrutinize power distribution synchro-waveform measurements," *IEEE Trans. Power Syst.*, early access, May 2021.

[7] *Intelligent Power System Recorder*. Accessed: Aug. 2020. [Online]. Available: https://www.candura.com/products/ipsr.html

[8] B. Gao, R. Torquato, W. Xu, and W. Freitas, "Waveform-based method for fast and accurate identification of subsynchronous resonance events," *IEEE Trans. Power Syst.*, vol. 34, no. 5, pp. 3626–3636, Sep. 2019.

[9] H. Mohsenian-Rad, E. Stewart, and E. Cortez, "Distribution synchrophasors: Pairing big data with analytics to create actionable information," *IEEE Power Energy Mag.*, vol. 16, no. 3, pp. 26–34, May/Jun. 2018.

[10] M. Farajollahi, A. Shahsavari, E. M. Stewart, and H. Mohsenian-Rad, "Locating the source of events in power distribution systems using micro-PMU data," *IEEE Trans. Power Syst.*, vol. 33, no. 6, pp. 6343–6354, Nov. 2018.

[11] S. Kulkarni, S. Santoso, and T. A. Short, "Incipient fault location algorithm for underground cables," *IEEE Trans. Smart Grid*, vol. 5, no. 3, pp. 1165–1174, May 2014.

[12] T. Takagi, Y. Yamakoshi, M. Yamaura, R. Kondow, and T. Matsushima, "Development of a new type fault locator using the one-terminal voltage and current data," *IEEE Trans. Power App. Syst.*, vol. PAS-101, no. 8, pp. 2892–2898, Aug. 1982.

[13] X. Yang, M.-S. Choi, S.-J. Lee, C.-W. Ten, and S.-I. Lim, "Fault location for underground power cable using distributed parameter approach," *IEEE Trans. Power Syst.*, vol. 23, no. 4, pp. 1809–1816, Nov. 2008.

[14] R. Krishnathevar and E. E. Ngu, "Generalized impedance-based fault location for distribution systems," *IEEE Trans. Power Del.*, vol. 27, no. 1, pp. 449–451, Jan. 2012.

[15] X. Wang *et al.*, "Location of single phase to ground faults in distribution networks based on synchronous transients energy analysis," *IEEE Trans. Smart Grid*, vol. 11, no. 1, pp. 774–785, Jan. 2020.

[16] Q. Cui and Y. Weng, "Enhance high impedance fault detection and location accuracy via μ-PMUs," *IEEE Trans. Smart Grid*, vol. 11, no. 1, pp. 797–809, Jan. 2020.

[17] M. M. Alamuti, H. Nouri, R. M. Ciric, and V. Terzija, "Intermittent fault location in distribution feeders," *IEEE Trans. Power Del.*, vol. 27, no. 1, pp. 96–103, Jan. 2012.

[18] C. Kim, T. Bialek, and J. Awiylika, "An initial investigation for locating self-clearing faults in distribution systems," *IEEE Trans. Smart Grid*, vol. 4, no. 2, pp. 1105–1112, Jun. 2013.

[19] H. Nouri, M. M. Alamuti, and M. Montakhab, "Time-based fault location method for LV distribution systems," *Elect. Eng.*, vol. 98, pp. 87–96, Mar. 2016.

[20] W. Zhang, X. Xiao, K. Zhou, W. Xu, and Y. Jing, "Multicycle incipient fault detection and location for medium voltage underground cable," *IEEE Trans. Power Del.*, vol. 32, no. 3, pp. 1450–1459, Jun. 2017.

[21] A. R. Herrera-Orozco, A. S. Bretas, C. Orozco-Henao, L. U. Iurinic, and J. Mora-Flóreze, "Incipient fault location formulation: A time-domain system model and parameter estimation approach," *Int. J. Elect. Power Energy Syst.*, vol. 90, pp. 112–123, Sep. 2017.

[22] A. S. Bretas, A. R. Herrera-Orozco, C. A. Orozco-Henao, L. U. Iurinic, and J. Mora-Flóreze, "Incipient fault location method for distribution networks with underground shielded cables: A system identification approach," *Int. Trans. Elect. Energy Syst.*, vol. 27, no. 12, pp. 1–19, Oct. 2017.

[23] L. A. da Costa, D. S. Gazzana, R. C. Leborgne, and D. W. P. Thomas, "Incipient fault location in underground distribution networks using electromagnetic time reversal," in *Proc. IEEE Int. Conf. Environ. Elect. Eng. Ind. Commer. Power Syst. Eur. (EEEIC / I&CPS Europe)*, Madrid, Spain, 2020, pp. 1–6.

[24] H. Khani, M. Moallem, S. Sadri, and M. Dolatshahi, "A new method for online determination of the location of switched capacitor banks in distribution systems," *IEEE Trans. Power Del.*, vol. 26, no. 1, pp. 341–351, Jan. 2011.

[25] K. Hur and S. Santoso, "On two fundamental signatures for determining the relative location of switched capacitor banks," *IEEE Trans. Power Del.*, vol. 23, no. 2, pp. 1105–1112, Apr. 2008.

[26] S. Xiong, Y. Liu, J. Fang, J. Dai, L. Luo, and X. Jiang, "Incipient fault identification in power distribution systems via human-level concept learning," *IEEE Trans. Smart Grid*, vol. 11, no. 6, pp. 5239–5248, Nov. 2020.

[27] P. D. Achlerkar, S. R. Samantaray, and M. S. Manikandan, "Variational mode decomposition and decision tree based detection and classification of power quality disturbances in grid-connected distributed generation system," *IEEE Trans. Smart Grid*, vol. 9, no. 4, pp. 3122–3132, Jul. 2018.

[28] A. J. Wilson, D. R. Reising, R. W. Hay, R. C. Johnson, A. A. Karrar, and T. D. Loveless, "Automated identification of electrical disturbance waveforms within an operational smart power grid," *IEEE Trans. Smart Grid*, vol. 11, no. 5, pp. 4380–4389, Sep. 2020.

[29] Y. Hu, W. Wu, and B. Zhang, "A fast method to identify the order of frequency-dependent network equivalents," *IEEE Trans. Power Syst.*, vol. 31, no. 1, pp. 54–62, Jan. 2016.

[30] M. L. Crow and A. Singh, "The matrix pencil for power system modal extraction," *IEEE Trans. Power Syst.*, vol. 20, no. 1, pp. 501–502, Feb. 2005.

[31] M. H. J. Bollen, E. Styvaktakis, and I. Y.-H. Gu, "Categorization and analysis of power system transients," *IEEE Trans. Power Del.*, vol. 20, no. 3, pp. 2298–2306, Jul. 2005.

[32] D. J. Trudnowski, J. M. Johnson, and J. F. Hauer, "Making prony analysis more accurate using multiple signals," *IEEE Trans. Power Syst.*, vol. 14, no. 1, pp. 226–231, Feb. 1999.

[33] W. Kersting, *Distribution System Modeling and Analysis*. Boca Raton, FL, USA: CRC Press, 2002.

[34] *Ver. 4.2 PSCAD/EMTDC (Software Package)*, Manitoba HVDC Res, Centre, Winnipeg, MB, Canada, Feb. 2010.
[35] T. E. Browne, "Practical modeling of the circuit breaker arc as a short line fault interrupter," *IEEE Trans. Power App. Syst.*, vol. PAS-97, no. 3, pp. 838–847, May 1978.
[36] G. I. Ospina, D. Cubillos, and L. Ibanez, "Analysis of arcing fault models," in *Proc. IEEE/Power Energy Soc. Transm. Distrib. Conf. Exposit.*, Bogota, Colombia, 2008, pp. 1–5.
[37] J. V. Milanovic, K. Yamashita, S. M. Villanueva, S. Ž. Djokic, and L. M. Korunović, "International industry practice on power system load modeling," *IEEE Trans. Power Syst.*, vol. 28, no. 3, pp. 3038–3046, Aug. 2013.

Milad Izadi (Student Member, IEEE) received the B.Sc. degree in electrical engineering from Razi University, Kermanshah, Iran, in 2015, and the M.Sc. degree in electrical engineering from the Sharif University of Technology, Tehran, Iran, in 2017. He is currently pursing the Ph.D. degree in electrical engineering with the University of California at Riverside, Riverside, CA, USA, where he is a Bonnie Reiss Carbon Neutrality Initiative Fellow. His research interests include power system monitoring and situational awareness, power system reliability, and data analysis. He is specifically working on applications of an emerging class of smart grid sensors, called waveform measurement units, and phasor measurement units in power distribution systems. He was the recipient of the 2019 Best Master Thesis Award from the Smart Grid Conference in Iran. He was on the list of the 2019 Best Reviewer of the IEEE TRANSACTIONS ON SMART GRID.

Hamed Mohsenian-Rad (Fellow, IEEE) received the Ph.D. degree in electrical and computer engineering from the University of British Columbia, Vancouver, BC, Canada, in 2008. He is currently a Professor of Electrical Engineering and a Bourns Family Faculty Fellow with the University of California at Riverside, Riverside, CA, USA. He has authored the textbook *Smart Grid Sensors: Principles and Applications* (Cambridge University Press, 2021). His research is on monitoring, data analysis, and optimization of power systems and smart grids. He was a recipient of the National Science Foundation CAREER Award, the Best Paper Award from the IEEE Power and Energy Society General Meeting, and the Best Paper Award from the IEEE Conference on Smart Grid Communications. He has been the PI on over ten million dollars research grants in the field of smart grid. He has served as an Editor for the IEEE TRANSACTIONS ON SMART GRID and the IEEE POWER ENGINEERING LETTERS.